Effects of metal impurities on the optical properties of polyethylene in the warm dense-matter regime

D. A. Horner, J. D. Kress, and L. A. Collins
Theoretical Division, Los Alamos National Laboratory, Los Alamos, New Mexico 87545, USA
(Received 8 March 2010; revised manuscript received 6 May 2010; published 3 June 2010)

For the warm dense-matter regime, we have examined the effects on the equation of state, conductivity, and optical properties of the introduction of a metal impurity (Al) into a poorly conducting mixture (CH_2) by means of quantum molecular-dynamics simulations employing temperature-dependent density-functional theory for temperatures between 1 and 4 eV and densities from ambient solid to a few times compressed. The properties such as dc conductivity and Rosseland mean opacity exhibit significant departures from the pure CH_2 results only for metal concentrations above about 50%. The system is representative of a wide range of environments that include planetary interiors, inertial confinement fusion capsules, and laser-produced plasmas.

DOI: 10.1103/PhysRevB.81.214301 PACS number(s): 52.65.Yy, 52.25.Vy, 61.20.Ja

I. INTRODUCTION

Impurities play a vital role in the behavior of materials from dilute gases to compressed solids. A small amount of dopant can radically alter the conductive properties of a semiconductor in the same manner in which a sprinkling of heavy ions can cool a hot, magnetically confined hydrogen plasma. While the effects of impurities have received considerable attention in many areas, their importance in the realm of warm dense-matter (WDM) has yet to receive a thorough investigation. This regime, which ranges in temperatures from a few thousand ($\sim$1 eV) to a few million ($\sim$100 eV) degrees kelvin and in densities from a few hundreds solid ($\sim 10^{21}$ atoms/cm^3) to hundreds of times compressed solid ($\sim 10^{25}$ atoms/cm^3), encompasses a diverse set of environments and phenomena such as the interiors of planets,[1,2] the atmospheres of white dwarfs,[3] the compression phase of an inertial confinement fusion (ICF) capsule,[4] and the plasma produced in the interaction of an ultrafast, high-intensity laser pulse with a solid.[5,6] For example, contaminants such as silicates, iron, and carbon within the basically hydrogen/helium interiors of jupiter and saturn influence the intrinsic composition and structure of these gas giants, in particular, the content or even existence of a solid rocky or icy core.[7] To model the vast range in masses, sizes, and environments of the ever-growing list of exoplanets[8,9] requires a more detailed understanding of the basic interplay of the bulk constituents with the impurities, especially given the ability now to probe the basic composition.[10] In a more terrestrial setting, the mixing of impurities from the capsule shells into the deuterium/tritium fuel can have a considerable impact on the ICF burn efficiency.[11,12] The evolution of capsule design from layers of hydrocarbon foams and heavy metals to simple shells of plastics such as polyethylene (PE) or light metals as beryllium has not altered the effects impurities can have on the basic behavior of the fuel. For example, the inclusion of small amounts of germanium in the plastic shell can damp certain hydrodynamical instabilities. In each of these examples, the accuracy of the macroscopic modeling of these environments rests strongly on a detailed knowledge of the underlying microscopic properties such as electrical conductivity, opacity, and equation of state (EOS).

The above-delineated environments cover a diverse collection of species and conditions. As a *representative system*, we seek a mixture of moderately light components with poor conductivity to which a heavier metal contaminant is added. The plastic PE, consisting at ambient solid density of long chains of CH_2, provides a suitable candidate for the former and aluminum for the latter. We examine such properties as the electrical conductivity and the mean opacity as a function of the metal content in the WDM regime at up to a few times the ambient solid density ($\sim$1 g/cm^3) and temperatures up to 50 000 K [$\sim$4 eV]. For these conditions, the PE (CH_2) forms a partially dissociated fluid. We modeled this system through large scale, highly sophisticated quantum molecular-dynamics (QMD) simulations, which treated the electrons quantum mechanically through finite-temperature density-functional theory (FTDFT) and the nuclei classically. This approach has proven highly effective in treating mixtures such as LiH,[13,14] H_2O,[15] HeH,[16] and AuAl (Ref. 17) in the WDM regime so that its extension to the addition of impurities is straightforward.[18] In the next section, we present an overview of the formalism and parameters employed in the simulations, followed by a presentation of the results.

II. FORMALISM

We have performed QMD simulations for a carbon-hydrogen-aluminum mixture having a fixed number of electrons N_e and ions N_i in a periodically replicated box of length $L(V \equiv L^3)$. In these simulations, the electrons receive a fully quantum mechanically treatment through solving the Kohn-Sham (KS) equations for a set of orbitals ψ_i and energies ϵ_i within a plane-wave, FTDFT formulation using the Vienna *ab initio* simulation package (VASP).[19–21] The ions evolve by classical molecular dynamics according the forces from the electron density and the ion-ion repulsion. Local thermodynamic equilibrium pertains with the electron and ion temperatures set equal ($T_e = T_i$). The electron temperature was fixed in the FTDFT and the ion temperature was kept constant through simple velocity rescaling. These conventions define a isokinetic ensemble (NVT) with a fixed number

$(N=N_e+N_i)$ of particles, volume, and temperature. All simulations employed only Γ point ($\mathbf{k}=0$) point sampling of the Brillouin zone. We solved the KS equations within the generalized gradient approximation (Perdew-Wang 91) and described the ion-electron interaction by projector augmented wave pseudopotentials for carbon, aluminum, and hydrogen with, respectively, four, three, and one valence electrons and maximum energy cutoffs ($E_{\max}$) of 700 eV, 400 eV, and 700 eV. A sufficient number of bands (states) n_b, typically 1000–2000, was included so that the occupation of the highest band was less than 10^{-3}. MD trajectories were generally evolved for 0.5 ps with time steps of 0.5 fs.

For this report, we concentrate on the optical properties of the medium and consider, in particular, the behavior of the dc conductivity $\sigma_{\rm dc}$ and the Rosseland mean opacity (RMO) κ_R as convenient gauges although we shall also employ the electronic or excess pressure P_e and internal energy U to assess the equation of state. The dc conductivity probes the low-frequency regime while the RMO emphasizes a region around the maximum of the absorption. The combination provides a broad indication of the trends in the behavior of the fluid with increased metal content.

The real part of the frequency-dependent conductivity $\sigma(\omega)=\sigma_1(\omega)+i\sigma_2(\omega)$ provides the basic information for computing these properties[22–24]

$$\sigma_1(\omega) = \frac{2\pi}{\Omega}\sum_{i,j} F_{ij}|D_{ij}|^2\delta(\epsilon_i - \epsilon_j - \omega), \tag{1}$$

where Ω is the atomic volume, F_{ij} is the difference between the Fermi-Dirac distribution at temperature T, and D_{ij} is the velocity dipole matrix element $|\langle\psi_i|\nabla|\psi_j\rangle|^2$. Substituting a narrow Gaussian of width Δ for the delta function permits a systematic determination of the real part of the conductivity; a Kramers-Kronig relation defines the imaginary part in terms of σ_1. The zero-frequency limit of the real part gives the dc conductivity $[\sigma_{\rm dc}=\sigma_1(0)]$. Other optical properties such as the index of refraction, the reflectivity, the dielectric function, and the absorption derive exclusively from a knowledge of the complex electrical conductivity. In particular, the absorption coefficient $\alpha(\omega)=\frac{4\pi}{n(\omega)}\sigma_1(\omega)$ with $n(\omega)$ the real part of the index of refraction from which derives the Rosseland mean opacity κ_R as

$$\frac{1}{\kappa_R} = \int_0^\infty \frac{B'(\omega)}{\alpha(\omega)}d\omega, \tag{2}$$

where $B'(\omega)$ is the derivative with respect to temperature of the normalized Planck's function. Given that the function B' peaks around $4k_BT$, the computed opacities exhibit the greatest sensitivity to the absorption coefficient around this energy. Since the conductivity depends on transitions between occupied and unoccupied orbitals, generally three to four times as many bands are required for convergence in contrast to the force. We find that averaging σ_1 over five to ten MD snap shots at times separated by a correlation length, proves sufficient to converge the optical properties within better than 5%. We generally report the frequency-dependent quantities in terms of the photon energy $(E=\hbar\omega)$.

From only a knowledge of the dc electrical conductivity, we can estimate the electronic thermal conductivity K_e by employing the Wiedemann-Franz law,[25]

$$K_e = L_0\sigma_{\rm dc}T_e, \tag{3}$$

where $L_0=\frac{\pi^2k_B^2}{3e^2}$ with k_B, the Boltzmann constant and e, the electron charge. This particular choice of the Lorenz factor L_0 best represents metallic systems and should apply better to cases of higher Al content. While this form yields a general range for the thermal conductivity over the conditions explored here, more quantitative results obtain from constructing the Onsager kinetic coefficients $\mathcal{L}_{ij}$ from Kubo formulas[26] resembling Eq. (1).

Our initial reference system consists of CH_2 molecules randomly distributed in a volume L^3 to form a disordered collection of N_C carbon atoms and N_H hydrogen atoms $[N_H=2N_C]$. We examine the effects of introducing a metallic impurity by systematically replacing the CH_2 units with aluminum atoms so that the total number $N_h[=N_C+N_{\rm Al}]$ of atoms of the heavy species, carbon and aluminum, remains constant. Isolated CH_2 has a carbon-hydrogen bond length of 1.07 Å and an aluminum atom, a radius of 1.25 Å. However, since the size of a CH_2 molecule does not precisely match that of Al atom, we have found that a direct replacement can lead in some cases to particles having anomalously close separations in the initial configuration. If the QMD commences with this situation, overly hot hydrogen atoms and condensed CH can result. To rectify this problem, we begin the MD simulation with a consecutive series of short propagations (~100–200 time steps) with the velocities rescaled at the end of each. This prescription allows all particles to settle into the proper relative configuration from which the long simulation can begin.

We consider two cases with $N_h=75$ and 150, which for pure CH_2 gives a total number of particles of 225 and 450, respectively. We report results in terms of the mass density of the pure CH_2 fluid $\rho=\frac{m_HN_H+m_CN_C}{L^3}$ and the fraction of Al, $f_{\rm Al}=\frac{N_{\rm Al}}{N_h}$. For example, a case with $N_C=N_h=75$ and $\rho=1$ g/cm^3 gives $L=12.04$ Å. A sample of pure Al ($f_{\rm Al}=1$) of 75 atoms at the same volume yields a density of 1.92 g/cm^3. We examine cases for initial CH_2 densities between 1 and 3 g/cm^3 and temperatures ranging from 1 to 4 eV, which track in a general sense the evolution of the early stages of ICF capsule compression.[27]

III. RESULTS AND DISCUSSION

Since experimental data does not exist in the WDM regime under investigation, we compare at various limits. First, for pure Al, we have reproduced the theoretical electrical conductivity results of Mazevet *et al.*,[28] which in turn agree very well with exploding wire experiments[29] at temperatures between 1 and 3 eV and Al densities from 0.02 to 2 g/cm^3. Second, for polyethylene $[CH_2]$ fluids, we compared in Fig. 1 against experimental Hugoniot results at densities between 1 and 2 g/cm^3 and temperatures of a few thousand kelvin. We performed NVT QMD simulations varying the temperature until the two sides of the Rankine-Hugoniot equation[30]

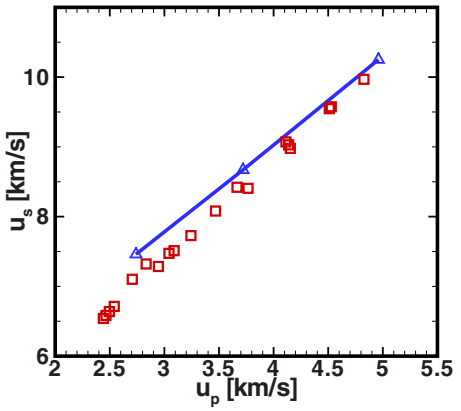

FIG. 1. (Color online) Comparison of CH_2 Hugoniot for QMD (blue; solid triangle) and experiment (Ref. 32) (red squares) in the shock velocity (u_s) and particle velocity (u_p) space.

agreed, thereby determining a pressure P and internal energy U and in turn the shock u_s and particle u_p velocities,[31] which agree to within better than 10% with data from shock experiments.[32] A more comprehensive study of the PE Hugoniot has recently appeared[33] that further demonstrates the efficacy of DFT methods for polymer systems.

We first consider the effects of the impurity on the EOS of the polyethylene fluid by examining in Fig. 2 the behavior of the electronic pressure P_e as a function of the Al fraction for several temperatures and densities. The pressure shows a very small increase in atmost 20% from pure CH_2 to pure Al. Since the components have similar sizes, replacing a CH_2 with an Al will not significantly alter the basic structure. While quantum mechanically, we substitute more complex entities, one having six valence electrons with one having three, the insensitivity of the pressure indicates that the resulting electronic structures behave in a similar manner. As we shall discover, this behavior does not translate to the optical properties. In fact this weak dependence on the Al fraction exhibited by the pressure masks, especially at the higher densities and temperatures, a more complex structure for the fluid. Examination of the pair-correlation functions, which give the probability of finding one species at a particular distance from another, indicates some breakage of the C-H bonds and the formation of short carbon chains (C-C) and of molecular hydrogen (H_2) and aluminum (Al_2).

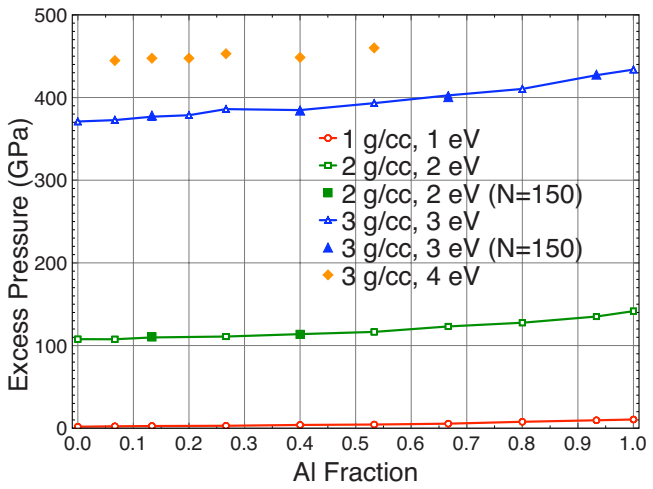

FIG. 2. (Color online) Electronic (excess) pressure for a CH_2/Al mixture as a function of the fraction of Al for 1 g/cm^3 and 1 eV (red circles); 2 g/cm^3 and 2 eV (green squares); 3 g/cm^3 and 3 eV (blue triangles); and 3 g/cm^3 and 4 eV (orange diamonds) for two values of N_h=75 (open symbols) and 150 (solid symbols).

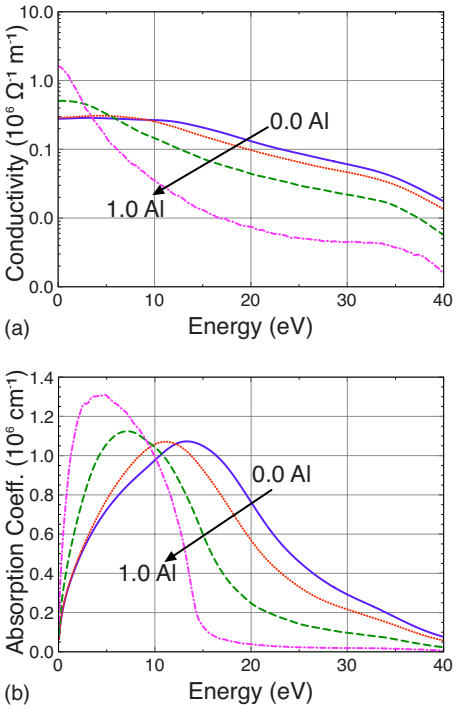

FIG. 3. (Color online) Comparison of the energy (frequency)-dependent electrical conductivity $\sigma_1(E)$ (left panel) and absorption coefficient $\alpha(E)$ (right panel) as a function of photon energy (E) at 1 g/cm^3, 1 eV, and N_h=75 for several Al fractions (f_{Al}=): 0.0 (solid/blue); 0.25 (dash/red); 0.75 (dot/green); and 1.0 (dash dot/violet).

We begin our investigation of the optical properties by examining the behavior of the energy-dependent electrical conductivity $\sigma_1(E)$ and absorption coefficient $\alpha(E)$ as a function of the metal concentration f_{Al} for the representative case of an initial PE density of 1 g/cm^3 at a temperature of 1 eV and N_h=75. As displayed in the left-hand panel of Fig. 3, the conductivity for the pure CH_2 behaves like a poor metal or semiconductor peaking at a nonzero value of the frequency and falling slightly at the origin with a dc conductivity of 0.3×10^6 $(\Omega\ m)^{-1}$ in contrast to a value for pure solid Al at ambient conditions of 38×10^6 $(\Omega\ m)^{-1}$. For small amounts of Al, $\sigma_1(E)$ continues to resemble the pure CH_2 result. After the fraction reaches about 0.5, the low-energy portion increases rapidly, resembling more the behavior of a metal. At these high concentrations, the Al atoms can readily share their electrons and significantly alter the conductive properties of the medium. In fact, for Al fractions greater than 0.65, the electrical conductivity for photon energies below 10 eV fits well to the Drude form of a simple metal.[28] As indicated by the right-hand panel in Fig. 3, the absorption coefficient shows a more gradual evolution from pure PE to Al. The maximum moves steadily to lower frequencies as the mag-

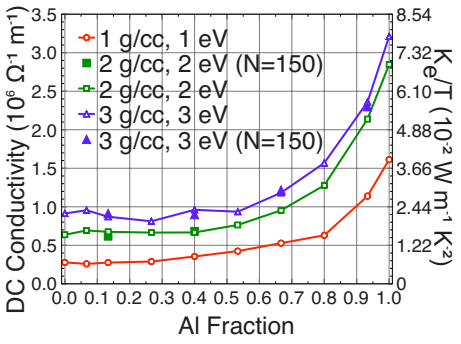

FIG. 4. (Color online) dc electrical conductivity for a CH_2/Al mixture as a function of the fraction of Al for 1 g/cm^3 and 1 eV (red circles); 2 g/cm^3 and 2 eV (green squares); and 3 g/cm^3 and 3 eV (blue triangles) for two values of N_h=75 (open symbols) and 150 (solid symbols). The plot also gives the electronic thermal conductivity divided by temperature $[K_e/T]$ as read from the right-hand ordinate scale.

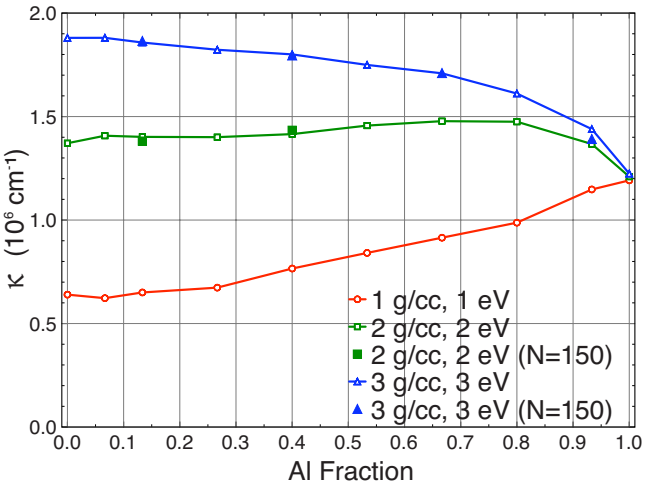

FIG. 5. (Color online) Comparison of Rosseland mean opacity as a function of temperature, density, and Al fraction. Labels same as Fig. 2.

nitude grows. This would indicate an increasing opacity with Al concentration since the Rosseland depends primarily on the behavior of the absorption coefficient around $4k_BT$ (4 eV in this case). We now turn to an examination of the mean opacity and dc conductivity to gain a broader perspective of the basic trends with changes in composition.

In Fig. 4, we display the dc conductivity as a function of temperature and density as the fraction of the metal content. The trend with f_{Al} found for 1 g/cm^3 and 1 eV also persists at higher densities and temperatures with a slowly increasing conductivity, essentially that of pure PE, up to a concentration of about 50% Al and a more rapid rise beyond 70%. The denser and hotter cases have an overall larger conductivity. We have compared calculations with N_h=75 and 150 C+Al atoms and find no size effects with the results within a few percent. Speculation exists on the possibility of small metal impurity concentrations causing significant changes in the opacity properties of the constituent material. At least for this case, we find no pronounced effects for low metal fractions. The system must reach about a 50% blend before noticeable changes occur in the conductivity. We have also performed calculations for a small number [1-3] of gold atoms in a CH_2 fluid and found little change in the basic optical properties. The evolution of macroscopic systems such as an ICF capsule may produce regions with far greater concentrations of the metal impurity than found in the initial sample; this situation could alter the basic transmission properties of the media. For completeness, we also plot in Fig. 4 the thermal conductivity determined from the Wiedemann-Franz law as a function of Al fraction. Since K_e/T for this rule scales as σ_{dc}, the trend simply follows the dc electrical conductivity.

In Fig. 5, we make a similar comparison for the RMO. In this case, a clear difference arises between the lowest and the two higher temperature-density cases. For the former, the opacity steadily rises as the Al concentration increases. On the other hand, for the latter, the opacity remains nearly level to concentrations of 70% and then falls as the system becomes pure Al. The right-hand panel in Fig. 3 gives insight into this behavior for the 1 g/cm^3 case. The main contribution to κ_R comes from photon energies around 4 eV. For all the concentrations, this position lies in a region of monotonically increasing absorption. As the Al fraction rises, the peak of the absorption curve increases in magnitude in this region, thus resulting in a smoothly growing RMO with increasing f_{Al}. For the higher temperatures, the RMO maxima (photon energies of 8 eV and 12 eV for 2 g/cm^3 and 3 g/cm^3, respectively) lie near the center of the absorption curve for all but the highest concentrations. In this case, the RMO remains basically constant as the Al concentration increases. The main contribution for the highest concentrations moves to the high-energy tail of $\alpha(E)$, which decreases with photon energy. This explains the decreasing values of the RMO for $f_{\mathrm{Al}} \rightarrow 1$. Again, the effects on the opacity due to the metal only appear at high concentrations.

For the warm dense-matter regime, we have examined the effects on the conduction and optical properties by the introduction of a metal impurity (Al) into a poorly conducting mixture (CH_2) by means of quantum molecular-dynamics simulations employing temperature-dependent density-functional theory. The properties such as dc conductivity and Rosseland mean opacity exhibit significant departures from the pure CH_2 results only for metal concentrations above about 50%. This has ramifications for macroscopic systems such as planetary interiors, inertial confinement fusion capsules, and laser-produced plasmas.

ACKNOWLEDGMENTS

We wish to acknowledge useful conversations with and information regarding ICF conditions from Guy Dimonte at Los Alamos as well as Al parameters from Michael Desjarlais at Sandia. We also thank Thomas Mattson of Sandia for sending us a preprint of Ref. 33. The Los Alamos National Laboratory is operated by Los Alamos National Security, LLC for the National Nuclear Security Administration of the U.S. Department of Energy under Contract No. DE-AC52-06NA25396.

[1] N. Santos, W. Benz, and M. Mayor, Science **310**, 251 (2005).
[2] A. Burrows, Nature (London) **433**, 261 (2005).
[3] G. Fontaine, P. Brassard, and P. Bergeron, Publ. Astron. Soc. Pac. **113**, 409 (2001).
[4] J. Paiser, J. Boyes, S. Kumpman, W. Lowdermilk, and M. Soren, Laser Focus World **30**, 75 (1994).
[5] K. Widmann, T. Ao, M. Foord, D. Price, A. Ellis, P. Springer, and A. Ng, Phys. Rev. Lett. **92**, 125002 (2004).
[6] R. Ernstorfer, M. Harb, C. Hebeisen, G. Sciaini, T. Dartigalongue, and R. Miller, Science **323**, 1033 (2009).
[7] D. Saumon and T. Guillot, Astrophys. J. **609**, 1170 (2004).
[8] S. S. Vogt, R. Wittenmeyer, R. Butler, S. O'Toole, G. Henery, E. J. Rivera, S. Meschiari, G. Laughlin, C. G. Tinney, H. R. A. Jones, J. Bailey, B. D. Carter, and K. Batygin, Astrophys. J. **708**, 1366 (2010).
[9] J. E. Bailey, M. D. Knudson, A. L. Carlson, G. S. Dunham, M. P. Desjarlais, D. L. Hanson, and J. R. Asay, Phys. Rev. B **78**, 144107 (2008).
[10] M. Janson *et al.*, Astrophys. J. Lett. **708**, 1737 (1978).
[11] T. Sangster, R. Betti, R. Craxton, J. A. Delettrez, D. H. Edgell, L. M. Elasky, V. Y. Glebov, V. N. Goncharov, D. R. Harding, D. Jacobs-Perkins, R. Janezic, R. L. Keck, J. P. Knauer, S. J. Loucks, L. D. Lund, F. J. Marshall, R. L. McCrory, P. W. McKenty, D. D. Meyerhofer, P. B. Radha, S. P. Regan, W. Seka, W. T. Shmayda, S. Skupsky, V. A. Smalyuk, J. M. Soures, C. Stoeckl, B. Yaakobi, J. A. Frenje, C. K. Li, R. D. Petrasso, F. H. Séguin, J. D. Moody, J. A. Atherton, B. D. MacGowan, J. D. Kilkenny, T. P. Bernat, and D. S. Montgomery, Phys. Plasmas **14**, 058101 (2007).
[12] P. Amendt, C. Cerjan, A. Hamza, D. Hinkel, J. Milovich, and H. Robey, Phys. Plasmas **14**, 056312 (2007).
[13] D. A. Horner, J. D. Kress, and L. A. Collins, Phys. Rev. B **77**, 064102 (2008).
[14] D. A. Horner, F. Lambert, J. D. Kress, and L. A. Collins, Phys. Rev. B **80**, 024305 (2009).
[15] T. R. Mattsson and M. P. Desjarlais, Phys. Rev. Lett. **97**, 017801 (2006).
[16] J. Vorberger, I. Tamblyn, B. Militzer, and S. A. Bonev, Phys. Rev. B **75**, 024206 (2007).
[17] J. Clérouin, V. Recoules, S. Mazevet, P. Noiret, and P. Renaudin, Phys. Rev. B **76**, 064204 (2007).
[18] J. D. Kress, D. Horner, and L. A. Collins, in *Shock Compression of Condensed Matter*, edited by M. Elert, M. Furnish, W. Anderson, and W. Proud (AIP, New York, 2009), pp. 931–934.
[19] G. Kresse and J. Hafner, Phys. Rev. B **47**, 558 (1993).
[20] G. Kresse and J. Furthmuller, Comput. Mater. Sci. **6**, 15 (1996).
[21] G. Kresse and J. Furthmuller, Phys. Rev. B **54**, 11169 (1996).
[22] L. A. Collins, S. R. Bickham, J. D. Kress, S. Mazevet, T. J. Lenosky, N. J. Troullier, and W. Windl, Phys. Rev. B **63**, 184110 (2001).
[23] M. P. Desjarlais, J. D. Kress, and L. A. Collins, Phys. Rev. E **66**, 025401(R) (2002).
[24] S. Mazevet, L. A. Collins, N. Magee, J. Kress, and J. Keady, Astron. Astrophys. **405**, L5 (2003).
[25] V. Recoules and J. P. Crocombette, Phys. Rev. B **72**, 104202 (2005).
[26] V. Recoules, F. Lambert, A. Decoster, B. Canaud, and J. Clerouin, Phys. Rev. Lett. **102**, 075002 (2009).
[27] G. Dimonte (private communication).
[28] S. Mazevet, M. P. Desjarlais, L. A. Collins, J. D. Kress, and N. H. Magee, Phys. Rev. E **71**, 016409 (2005).
[29] A. W. DeSilva and J. D. Katsouros, Phys. Rev. E **57**, 5945 (1998).
[30] Y. Zeldovich and Y. Raiser, *Physics of Shock Waves and High Temperature Phenomena* (Dover Press, New York, 2002).
[31] The initial conditions were $P_0=0$, $U_0=-5.28$ eV/atom, and $\rho_0=0.916$ g/cm^3. For U_0, VASP calculations on isolated planar zigzig polyethylene chains $[CH_2]_n$ with $n=36$, 72, and 144 established an energy/CH_2 of 16.57 eV, corrected for the zero-point motion by 0.24 eV/atom.
[32] *LASL Shock Hugoniot Handbook*, edited by S. March (University of California, Berkeley, CA, 1998).
[33] T. R. Mattsson, J. M. Lane, K. R. Cochrane, M. P. Desjarlais, A. P. Thompson, F. Pierce, and G. S. Grest, Phys. Rev. B **81**, 054103 (2010).